Inelastic scattering of hydrogen atoms off pristine and hydrogen-covered W(100) surfaces

Raidel Martin Barrios, Oihana Galparsoro, Aliezer Martínez Mesa, Llinersy Uranga-Piña, Cédric Crespos, Pascal Larrégaray

Inelastic Scattering of Hydrogen Atoms off Pristine and Hydrogen-Covered W(100) Surfaces

Raidel Martin Barrios,[1,2,a] Oihana Galparsoro,[3,b] Aliezer Martínez Mesa,[2,4,c] Llinersy Uranga Piña,[2,4,d] Cedric Crespos,[1,e] and Pascal Larregaray[1,f]

[1] *Univ. Bordeaux, CNRS, Bordeaux INP, ISM, UMR 5255, F-33400, Talence, France*

[2] *DynAMoS (Dynamical processes in Atomic and Molecular Systems), Facultad de Física, Universidad de la Habana, Cuba*

[3] *Donostia International Physics Center (DIPC), Paseo Manuel de Lardizabal 4, 20018 Donostia-San Sebastián, Spain.*

[4] *Laboratoire Collisions Agrégats Réactivité (IRSAMC), Université Toulouse III - Paul Sabatier, UMR 5589, F-31062 Toulouse Cedex 09, France*

Recent experiments have shown that translational energy loss is mainly mediated by electron-hole pair excitations for hydrogen atoms impinging on clean metallic surfaces. Inspired by these studies, quasi-classical trajectory simulations are here performed to investigate the energy transfer after scattering of hydrogen atoms off clean and hydrogen-covered tungsten (100) surfaces. The present theoretical approach examines the coverage effect of the preadsorbed hydrogen atoms, as was done recently for the (110) crystallographic plane in *[J. Phys. Chem. C* ***125****, 14075 (2021)]*. As suggested, scattering can be described in terms of three different dynamical mechanisms, the contribution of which changes with coverage which allow to rationalize the shape of the energy loss spectra.

I. INTRODUCTION

The study of chemical reactions on solid substrates is a topic of current interest, owing chiefly to their relevance in technological processes such as heterogeneous catalysis, surface passivation, hydrogen storage, corrosion, chromatography, among others[1–5]. A detailed understanding of the microscopic mechanisms underlying chemical reactions at surfaces is a prerequisite for enhancing the efficiency of the associated applications. In spite of considerable effort devoted to the characterization of molecule-surface interactions, and of the energy redistribution mechanisms at the gas-solid interface[6,7], elucidating the influence of these factors on elementary reaction steps such as dissociative adsorption, diffusion, bond breaking and formation, and desorption, still poses significant challenges to modern surface science.

Notably, heterogeneous reactions involving hydrogen lie at the heart of several key technologies for large scale exploitation of renewable energy sources (namely hydrogen production via photocatalytic water splitting[8,9], hydrogen storage[10–12], and plasma-wall interactions in divertors of emerging ITER nuclear fusion reactors[13–17]), and of natural phenomena (for example, formation of interstellar molecular hydrogen[18]).

Over the past half-century, the molecular level knowledge on surface processes experienced significant progress. On the one hand, the advent and continuous progression of a variety of surface-sensitive experimental techniques (e.g., atomic and molecular beam scattering, low-energy electron diffraction, high resolution electron energy loss spectroscopy, scanning tunneling microscopy, sum frequency generation spectroscopy) provided access to a large body of microscopic information with unprecedented accuracy. On the other hand, molecular dynamics and Monte Carlo simulations evolved into powerful tools to rationalize experimental data, and to predict physico-chemical properties and reaction rates of gas-surface phenomena, sometimes beyond the experimentally accessible spatial, time, and energy resolutions. Atomic hydrogen (H) adsorption on metal surfaces, for example, has been intensively studied both theoretically and experimentally[19–23].

Recent combined atomic beam scattering experiments and molecular dynamics simulations have shown that the average energy losses of H atoms impinging on (111) planes of six *fcc* transition metals (viz. gold, platinum, silver, palladium, cooper, and nickel) exhibit a mild dependence on the specific chemical element[19,20]. These studies ruled out the charge transfer between hydrogen and the surface, and proven that energy dissipation is largely dominated by electron hole pair (ehp) excitations rather than coupling to surface phonons. This conclusion is further supported by recent molecular dynamics simulations of inelastic scattering of H atoms on gold (111) and tungsten (110) surfaces[24]. Moreover, the excitation of ehp was found to play a major role in the slowing down of hyperthermal difusion of hot hydrogen adatoms on tungsten substrates, thereby decreasing diatom recombination[25,26] at low collision energy. Tungsten (W) is a frequent subject of these investigations, as this material constitute a promising candidate for the fabrication of divertors of the forthcoming ITER nuclear

[a] rmartin@fisica.uh.cu
[b] oihana.galparsoro@ehu.eus
[c] aliezerm@gmail.com
[d] llinersy@gmail.com
[e] cedric.crespos@u-bordeaux.fr
[f] pascal.larregaray@u-bordeaux.fr

fusion reactor[13–17]. Although H atom adsorption on metals is a very efficient process, most experimental and simulated studies carried out to date have focused on atomic hydrogen scattering off clean metallic surfaces rather than H-covered substrates. Contrastingly, recent molecular dynamics simulations addressed the characterization of the energy losses of hydrogen atoms scattered on tungsten (110) substrates, as a function of surface coverage[27]. The question remains as to how the presence of adatoms influence the energy transfer in similar systems, e.g., for other metals or projectiles, and for different topologies of the tungsten surface. The distinct geometrical arrangement of tungsten atoms (and of the main adsorption sites for H adatoms) on the W(100) and the W(110) crystalographic planes, for example, markedly affects processes such as adsorption, dissociative chemisorption, and atom recombination[26,28–32]. Likewise, a significant influence of the symmetry of the exposed surface, on N_2 adsorption, was reported in simulations of molecular beam experiments on Fe(111)[33] and Fe(110)[34,35] solids.

The purpose of this paper is to investigate the translation inelasticity upon scattering of hydrogen atoms by clean and H-covered W(100) surfaces, and therefore to assess the effect of the modification of the surface symmetry on the energy transfer from the incoming atom into the solid. To this aim, we perform quasi-classical trajectory simulations including electronic friction, on a previously developed ground state potential energy surface[25,31].

The paper is organized as follows. In Section II, the theoretical model and the details of the molecular dynamics simulations of the inelastic scattering of H atoms on W(100) are described. In Section III, the characterization of the energy dissipated into the solid is presented and discussed in terms of the energy loss spectra of scattered atoms, and the distribution of distances of closest approach to the surface. The conclusions are briefly summarized in Section IV.

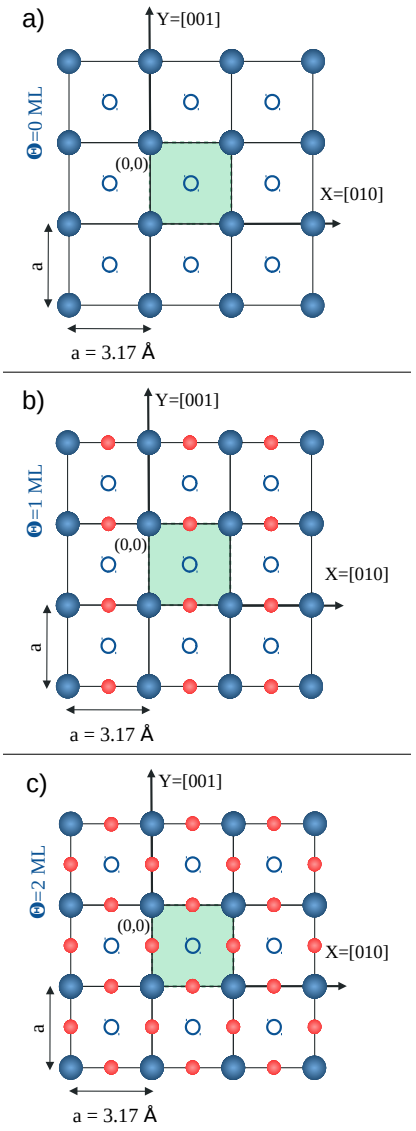

FIG. 1. Two-dimensional representation of a fragment of the W(100) surface, for three values of the surface coverage: Θ = 0 ML (panel a), Θ = 1 ML (panel b), and Θ = 2 ML (panel c). The lattice constant a is set to 3.17 Å. Solid and open blue circles indicate the positions of the first and the second layer of tungsten atoms, respectively. The sampling areas of initial positions (X_p,Y_p) of the projectiles are highlighted in green, and the equilibrium positions of the H adatoms are represented by solid red circles.

II. METHODOLOGY

A. Potential energy surface

Quasi-classical trajectory (QCT) simulations of H atom scattering have been carried out for the pristine W(100) surface (Θ = 0), and for two different values of the surface coverage (Θ = 1, 2 ML, expressed in monolayer (ML) unit). Trajectories are propagated on a Density Functional Theory (DFT) based, multiadsorbate potential energy surface (PES)[25,31], previously developed for the title system using an adaptation of the corrugation reducing procedure (CRP)[36,37], and within the frozen surface approximation. The latter approximation holds owing to the large mismatch between the masses of hydrogen and tungsten atoms (m_H/m_W = 1/183.5), which is expected to lead to negligible energy transfers to tungsten phonons[19,20].

DFT calculations were performed using the slab supercell approach, within the generalized gradient approximation and employing the PW91 functional[38,39] to describe electronic exchange and correlation.

Following Refs. 25 and 31, the potential energy surface (at finite coverages) is represented as a superposition of the the three-dimensional H/W(100) interaction potential, $V^{3D}(\mathbf{r}_i)$, and the six-dimensional diatomic interpo-

lation functions $I^{6D}(\mathbf{r}_i, \mathbf{r}_j)$[31,36], i.e.,

$$V(\{\mathbf{r}_i\}) = \sum_{i=1}^{N} V^{3D}(\mathbf{r}_i) + \sum_{i=1}^{N}\sum_{j>i}^{N} I^{6D}(\mathbf{r}_i, \mathbf{r}_j)\,. \quad (1)$$

In equation (1), $\mathbf{r}_i$ is the position vector of ith hydrogen atom, and the double summation runs over all pairs of H atoms. The PES (1) describes H penetration into the bulk down to -3.9 Å (the plane Z=0 is defined by the positions of tungsten atoms in the topmost layer).

The multiadsorbate PES accounts for one- and two body contributions to the interaction potential, whereas higher order contributions are ignored in the expansion (see eq. 1). Therefore, trajectories are stopped whenever one H atom approach closer than 1.5 Å from two neighbouring H atoms simultaneously. In the following results, the number of such events is found to be statistically irrelevant as only 0.5 % of these three-body encounters involve the projectile when considering atomic scattering on W(100).

B. Quasi-classical trajectory simulations

QCT calculations use a 6×6 square supercell with periodic boundary conditions in order to minimize finite-size effects, and to mimic an infinite surface (i.e., the basic $a \times a$ cell is replicated along the two perpendicular directions parallel to the metal surface). The origin of the reference frame is located on top of a tungsten atom, and the X, Y, Z axes lie respectively along the [010], [001] and [100] crystallographic directions.

The classical equations of motion are integrated for one projectile atom and 36 or 72 adsorbates (for coverages Θ = 1 ML, and Θ = 2 ML, respectively). The H-adsorbates initially sit at their equilibrium positions (in the *Bridge* site), and their total energy is set equal to the Zero Point Energy (ZPE). A schematic of the equilibrium positions of the adsorbates is displayed in figure 1. A detailed account of the adsorbed layer structure and energetics, and of the semiclassical procedure followed to assign the ZPE can be found elsewhere[25,26].

The projectile stands initially at $Z_p(t = 0) = 7.0$ Å from the tungsten surface, in the asymptotic region of the atom-substrate interaction potential. Concomitantly, the initial coordinates (X_p,Y_p) are randomly sampled in the irreducible unit cell of the covered surface (green areas in figure 1). In order to resemble experimentally relevant conditions[19], individual H atoms impinge the tungsten surface with a collision energy $E_i = 2.75$ eV. The incident atomic beam propagates in the direction defined by the polar angle $\theta_i = 45°$ (with respect to the Z[100] surface normal), and azimuthal angle $\phi_i = 0°$ (with respect to the X[010] axis). The energy losses of atoms scattered either in the whole space or in the specular direction ($\theta_{scat} = 45 \pm 5°$, $\phi_{scat} = 0 \pm 2°$) are analyzed.

To ensure the numerical convergence of the computed observables, more than 2 millions trajectories were run for each surface coverage up to a total integration time of 1 ps. It was checked that further increasing the integration time beyond 1 ps does not modify the results.

Energy dissipation via ehp excitations in the metal is modeled within the framework of the Local Density Friction Approximation (LDFA)[40,41]. In the electronic friction approach to H atom scattering, the equations of motion for the projectile and the adsorbates are augmented with dissipative and random forces. These forces mimic the effect of nonadiabatic energy transfer between the continuum of electronic states of the metal and the hydrogen atoms. The resulting Langevin equation reads:

$$m_H \ddot{\mathbf{r}}_i = -\frac{\partial V(\{\mathbf{r}_i\})}{\partial \mathbf{r}_i} - \eta_{el}(\mathbf{r}_i)\dot{\mathbf{r}}_i + \mathbf{F_L}(\mathbf{t}), \quad (2)$$

where m_H is the mass of a hydrogen atom. Equation (2) is integrated employing the explicit Beeman's algorithm.

First off, the friction force depends parametrically on the position $\mathbf{r}_i$ of the atom i, and it is proportional to the velocity of the atom. In the LDFA, the position-dependent friction coefficient $\eta_{el}(\mathbf{r}_i)$ corresponds to an atom embedded in a homogeneous free electron gas with the same electron density as the metallic substrate at the position $\mathbf{r}_i$[19,21,40,41]. Secondly, the random force $\mathbf{F_L}(\mathbf{t})$ incorporates the effect of electron temperature into equation (2), and it is taken here as a Gaussian white noise[41]. Electronic temperature is set to 300K. $\mathbf{F_L}(\mathbf{t})$ is connected to the frictional force by the second fluctuation-dissipation theorem. The random force contribution has been neglected in various molecular dynamics simulations with electronic friction, in the low- and intermediate-electronic temperature regimes, for example in the study of the relaxation of hot hydrogen atoms on clean metallic surfaces[42–44], or diatom recombination[25,26,45]. Nevertheless, random forces have been found to play a major role, for instance, in surface elementary processes triggered by intense laser pulses, causing electrons to be heated up to a few thousands of Kelvin[41,46–52]. Moreover, the random term noticeably influences the energy loss spectra of hydrogen atoms scattering off clean metal surfaces, even at room temperature[24,53]. The effect of energy dissipation to surface phonons is ignored here, due to the aforementioned predominance of energy transfer to ehp in the early relaxation of hydrogen on metals[19,20,42,43,54,55]. To prevent leakage of the ZPE, the friction force acts only when the energy of the preadsorbed atom exceeds the ZPE. Details can be found in Refs. 25 and 26.

To the purpose of computing the branching probability among the multiple reaction channels, the space is partitioned into three regions of interest: $Z \leq 0$ Å, $0 < Z \leq 7.0$ Å, and $Z > 7.0$ Å. The following elementary processes are considered: (i) *reflection* (or *atomic scattering*): whenever the impinging atom is reflected back to the initial altitude ($Z_p > 7.0$ Å), (ii) *abstraction*: if a H_2 molecule reaches a separation of 7.0 Å from the surface, (ii) *absorption*: if the projectile atom lies below the topmost layer of tungsten atoms (i.e., $Z \leq 0$ Å) at the end of the total integration time (1 ps), (iv) *adsorption*:

if the projectile atom lies between the levels Z =0 Å and Z = 7.0 Å at the end of the total integration time.

The probability of the impinging atom to get adsorbed while one initially adsorbed H atom gets desorbed was found to be marginal (e.g., less than 1.2% of the scattered trajectories for Θ= 2 ML).

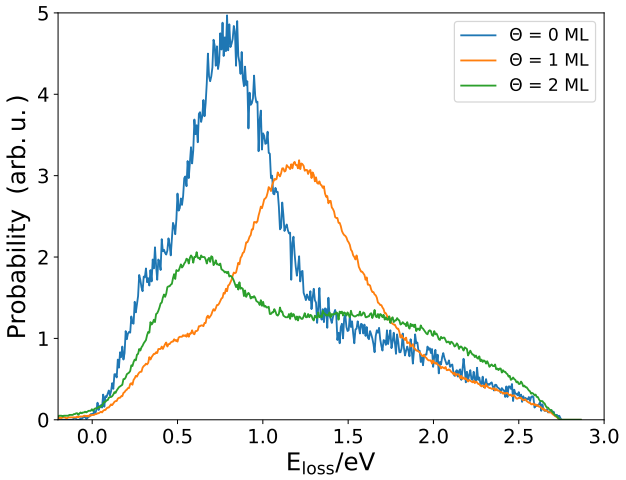

FIG. 2. Energy loss spectra of H atoms scattered off W(100) surface, in all directions, and for three selected values of the surface coverage: Θ = 0 ML (blue), 1 ML (orange), and 2 ML (green). The collision energy of E_i = 2.75 eV, temperature is set to T_s = 300 K, and the incident angles are $\varphi_i = 0°$, $\vartheta_i = 45°$. The areas under the different curves are normalized to the scattering probability.

III. RESULTS AND DISCUSSION

The energy loss spectra of H atoms undergoing inelastic scattering on W(100) surfaces are displayed in figure 2, for selected values of the surface coverage: Θ = 0 ML, 1 ML, and 2 ML. The spectra in figure 2 take into account the hydrogen atoms that are scattered off in all directions. The area under the curves have been normalized to the fraction of trajectories leading to H atom scattering, thus the plots represent the reduction of the scattering probability for increasing coverages, being respectively 0.66, 0.51, and 0.37, for Θ = 0 ML, 1 ML, and 2 ML. The observed depletion of the scattering probability can be rationalized in terms of the enhanced adsorption for covered surfaces, as a consequence of the addition of a very efficient dissipation mechanism by H adatoms. This trend is consistent with the results of previous simulations of hydrogen scattering dynamics on metal surfaces[25–27].

The energy loss distributions evolve from a shape consisting of a main peak (centered at E_{loss} = 0.80 eV, and 1.20 eV, for Θ = 0 ML, and 1 ML, respectively), an inner shoulder, and a outer, slowly decaying tail, into a double peak structure (with peaks centered at 0.6 eV, and at 1.6 eV, for Θ = 2 ML). The energy loss spectra for all scattered atoms is much more structured than for the (110) symmetry (see Fig. 2 of Ref.[27]). As suggested previously, the shape of the spectra can be also rationalized here in terms of underlying scattering mechanisms.

The probability distributions of first rebound altitudes for the scattered H are presented in figure 3 for Θ = 0 ML, 1 ML, and 2 ML. The distribution can be formally split into three contributions, corresponding roughly to the spatial regions $Z > 0.9$ Å, 0 Å$< Z < 0.9$Å, $Z < 0$ Å, and labelled here as *Top* (T), *Hollow-Bridge* (HB), and *Subsurface* (S), respectively. The insets display the position of the first rebounds onto the irreducible surface cell for zero coverage. For the clean W(100) surface, the T contribution corresponds to rebounds on top of the tungsten atom. The size of the S contribution indicates that a large fraction of reflected trajectories experiences the first turning point below the metal surface onto the tungsten atoms of the second layer (a small component around Z = -2.0 Å also scattered from below the first subsurface layer located at Z = -1.585 Å). There is also comparatively a lower contribution from scattering, in between the tungsten atoms at 0 Å$< Z <$ 1.2Å (HB).

Upon filling the *Bridge* adsorption sites (for Θ = 1 ML), the scattering from Z = -2 Å is removed. Concomitantly, there is a significant decrease of both the S and the HB contributions to reflection. Further increasing of coverage, (up to Θ = 2 ML) provokes an additional, marked depletion of the S and HB contributions, and a significant enhancement of T-type reflections (i.e., above Z = 0.9 Å). The kinetic energy loss distribution can be rationalized in terms of *Top* (T), *Hollow-Bridge* (HB), *Subsurface* (S) contributions. The resulting decomposition is shown in figure 4 for clean and H-covered W(100) surfaces. It allows to establish the link between the structure of the energy loss spectra and the distribution of altitudes of first rebounds. Typically, the T, HB, and S contributions consist of a maximum and a slowly decaying tail. For each component, the position of the maximum shifts to higher energies for increasing surface coverage, due to the presence of additional scatterers that render energy dissipation highly efficient. For the highest value of the surface coverage considered here (Θ = 2 ML), the reduced frequency of HB and S scattering events is accompanied by a noticeable increase of the T contribution.

A few differences and similarities with respect to the energy transfer on H-covered W(110) surfaces shed light onto the influence of surface symmetry on this process. For example, the overall scattering probability is nearly the same for the pristine W(100) and W(110) substrates (0.66 and 0.69, respectively). Likewise, the average energy loss is only slightly lower for the (100) surface (1.00 eV) than for the (110) surface (1.08 eV). Since the excitation of ehp is the only active dissipation channel for clean surfaces, the mildly reduced energy transfer can be understood in terms of the lower atomic density of

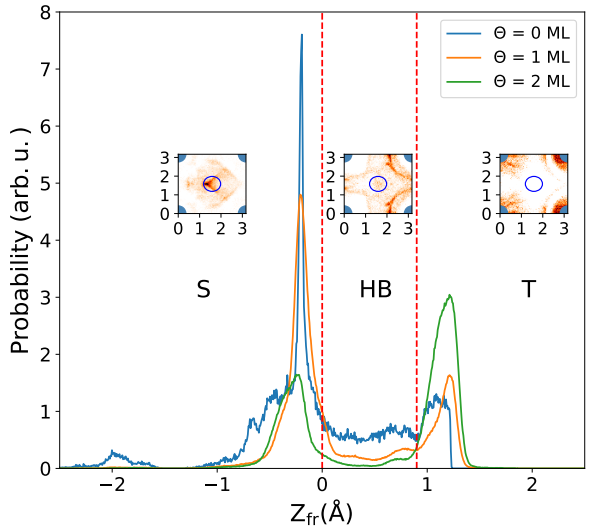

FIG. 3. Probability distribution of altitudes of the projectiles first rebound, Z_{fr}, for selected values of the surface coverage Θ = 0 ML (blue), 1 ML (orange), and 2 ML (green). The so-called T, HB, and S contributions correspond to first reflections in the spatial domains $Z_{fr} > 0.9$ Å, 0 Å$< Z_{fr} < 0.9$ Å, and $-$ 2.5 Å$< Z_{fr} <$ 0 Å, respectively. For these three contributions, the distributions of the (X,Y) coordinates of the projectile first rebound at zero coverage are displayed in the insets (distances in Å). In the insets, the darker the color, the higher the reflection probability. Blue solid circles points indicate the positions of the W surface atoms, whereas blue empty circles indicate the positions in the second layer of tungsten atoms.

the (100) surface. Indeed, scattering at three-fold hollow sites on the W(110) plane provides the leading contribution to the energy loss spectrum in this material[27]. The electron density at these sites, and thus energy dissipation within the framework of LDFA, is higher than that of bridge sites on the W(100) plane. However, this is partially compensated by the fact that the incoming H atom is allowed to get deeper into the W(100) solid, due to lower surface compacity, and therefore it experiences higher electron densities and electronic friction for a longer time.

Furthermore, it is striking that the main peak(s) in the energy loss spectra are more sharply defined for scattering off tungsten (100), than the corresponding maxima for the W(110) substrate. These differences are related to the distinct proportions of the T, HB and S mechanisms for both symmetries. For the pristine (100) surface, the energy loss spectrum mainly results from the T and S scattering which correspond to well separated energy loss. This is not the case for the pristine (110) surface for which the three mechanisms contribute in similar proportions to the scattering and span more uniformly the whole range of energy losses[27]. Noteworthy, for Θ = 2 ML and in the energy region $E_{loss} \gtrsim 1.9$ eV, the kinetic energy loss spectrum in figure 2 exhibits a sizable increase of the scattering probability, compared the very similar high-energy tails for the pristine and the 1 ML-covered surface.

The dependence of the average energy loss on the adsorbate concentration is non monotonous. The presence of hydrogen adatoms strengthens kinetic energy transfer from the projectile, and the average energy loss $\langle E_{loss} \rangle$ increases to 1.23 eV for a surface coverage of 1 ML. Nevertheless, $\langle E_{loss} \rangle$ reduces down to 1.21 eV for 2 ML, owing to the steep increase of the fraction of trajectories (57 %) which scatter upon direct collisions with tungsten atoms on the surface.

Summing up, when considering H atoms scattered off tungsten (100) surfaces in all directions, the average kinetic energy loss is larger for H-covered tungsten than for the clean surface. The enhanced energy transfer in presence of H adatoms, also leads to the decrease of the overall scattering probability, since the more efficient energy dissipation favours hydrogen sticking to the surface.

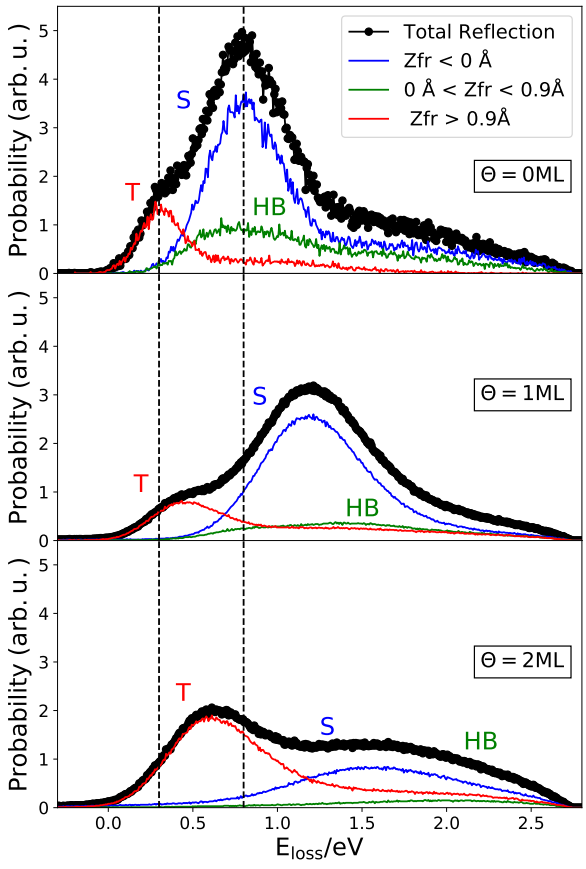

FIG. 4. Energy loss spectra for all scattered atoms (black solid circles), and their decomposition into T (red), HB (green), and S (blue) contributions. The panels display the results at different surface coverages: Θ = 0 ML (top), 1 ML (middle), and 2 ML (bottom). The vertical dashed lines indicate the positions of the maxima at zero coverage.

In figure 5, we focus on the energy loss distributions

for specular reflection of H atoms on the metal surface, as this is an usual observable of molecular beam scattering experiments[19,20]. For $\Theta = 0$ ML and 1 ML, the shapes of the energy loss distributions for specular reflection are qualitatively similar to those obtained by taking into account the scattering in all directions. However, regarding at all the coverages studied, two differences are worth to mention: the low-energy shoulder of each distribution is more prominent for the case of specular reflection, and the overall scattering probability is approximately 10% and 50% larger than for the pristine surface at $\Theta = 1$ ML and $\Theta = 2$ ML (respectively $8.23 \cdot 10^{-3}$ and $1.1 \cdot 10^{-2}$ as compared with $7.4 \cdot 10^{-3}$ for the pristine surface).

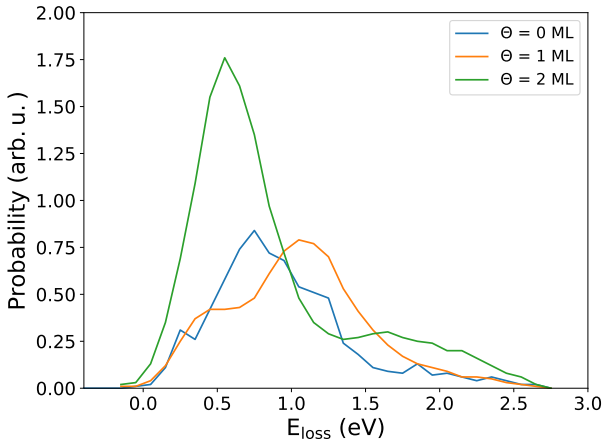

FIG. 5. Energy loss spectra of atoms undergoing specular reflection, for $\Theta = 0$ ML (blue), 1 ML (orange), and 2 ML (green). The collision energy of $E_i = 2.75$ eV, temperature is set to $T_s = 300$ K, and the incident angles are $\varphi_i = 0°$, $\vartheta_i = 45°$. The areas under the different curves are normalized to the scattering probability.

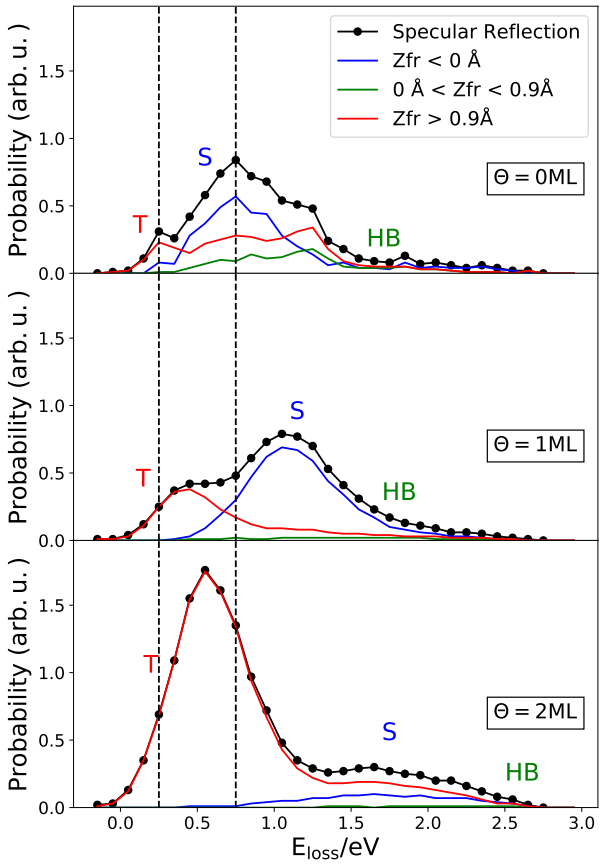

FIG. 6. Energy loss spectra for atoms scattered at specular angles (black solid circles), and their decomposition into T (red), HB (green), and S (blue) contributions. The panels display the results at different surface coverages: $\Theta = 0$ ML (top), 1 ML (middle), and 2 ML (bottom). The vertical dashed lines indicate the positions of the maxima at zero coverage.

The average energy loss upon specular scattering off H-covered surfaces also follows a similar trend as the reflection in all directions. The average energy dissipated into the solid increases from 0.94 eV (for the pristine surface) up to 1.04 eV (for $\Theta = 1$ ML), and subsequently it decreases down to 0.86 eV (for $\Theta = 2$ ML).

The contributions of T, HB, and S scattering to the energy loss distributions of atoms undertaking specular reflection on the W(100) plane are displayed in figure 6. It can be seen, that the energy loss spectra corresponding to T, HB, and S shift towards the higher energy values and broaden, as the adsorbate concentration gets larger. The relative contribution of each component also changes significantly.

The energy loss spectrum for subsurface specular reflections on pristine surfaces, for instance, has the same overall shape (after appropriate rescaling) as the corresponding distribution for scattering in all directions. To the contrary, the T and the HB contributions to total reflection consist chiefly of trajectories which, after the collision with the tungsten surface, are deflected away from the specular reflection direction. This is cleared up by the extensive depletion of T and HB peaks in the top panel of figure 6, compared to the case of total reflection (cf. figure 4, top panel).

For a H-coverage of 1 ML, the S component is predominant for incident atoms releasing an energy $E_{loss} \geq 0.7$ eV into the solid. Interestingly, the S and T components of the energy loss spectra have roughly the same shape as for the case of total reflection. For $\Theta = 2$ ML, the T contribution is predominant over the entire accessible energy range ($E_{loss} \leq 2.75$ eV), and it cause the spectrum to be strongly peaked at low energy transfers. Finally, the HB contribution changes from playing minor role for specular reflection on clean W(100) substrates, to almost vanish for H-covered surfaces. Up to our knowledge, a similar effect has not been reported in previous studies of the hydrogen scattering dynamics on metal surfaces.

To sum up, as for the (110) crystallographic plane, the specular scattering from the (100) plane can be rationalize in terms of three underlying scattering mechanisms.

Because of lower compacity, scattering from regions in between tungsten atoms (HB) is not favored and reflection occurs mainly after collision on top of tungsten surface atoms or off the first sublayer. For both symmetries, a great enhancement of specular scattering is observed with increasing coverage which originates from scattering off top tungsten atoms. Preliminary analyses point out a significant decrease of the corrugation in the region of the top site with increasing coverage. This issue is currently under detailed scrutiny.

IV. CONCLUSIONS

The scattering of hydrogen atom off clean and H-covered (100) tungsten surface has been analysed by means of the quasi-classical trajectory method accounting the electron-hole pair excitation of metal electrons. The analysis, confirms that the energy loss for all the scattered atoms is higher when the coverage is included than without it. The scattering probability decreases as a function of the coverage due to the efficient energy interchange between the projectile and adsorbed atoms. Besides, the scattering probability into the specular direction, increases with increasing coverage, accompanied by a decrease of the energy loss. This effect is particularly interesting, since current experimental techniques usually study scattering in a given plane rather than in the whole space. A shift towards high values of energy losses of the peaks of each underlying scattering contribution off *Top*, *Hollow-Bridge* and *Subsurface* sites is also observed as coverage increases. For the (100) surface, the *Hollow-Bridge* contribution to distribution of energy loss is less appreciable than in (110) surface, which is a direct consequence of the lower compacity resulting from the distribution of the surface atoms. Conversely, scattering from the sub surface is significant from low to moderate coverage.

Data Availability Statement

Data will be made available on reasonable request

Acknowledgements

The authors acknowledge the support of the French Embassy in Cuba, the University of Bordeaux, the CNRS and Erasmus Mundus program for funding and ISM and University of Bordeaux for providing computing resources. This work was conducted in the scope of the transborder joint Laboratory *Quantum-ChemPhys*: Theoretical Chemistry and Physics at the Quantum Scale (ANR-10-IDEX-03-02). This study has been partially supported by the European Union's Horizon 2020 research and innovation programme under the Marie Sklodowska-Curie grant agreement n^{o}898663 (A.M.M.), the EUR grant NanoX n° ANR-17-EURE-0009 in the framework of the Programme des Investissements d'Avenir (L.U.P.), and the APS-EPS-ICTP Travel Award Fellowship Programme (L.U.P.). O.G. acknowledges financial support by the Gobierno Vasco-UPV/EHU [Project No. IT1569-22]

[1] J. Greeley, J. K. Nørskov, and M. Mavrikakis, Annual review of physical chemistry **53**, 319 (2002).
[2] M. Bonn, S. Funk, C. Hess, D. N. Denzler, C. Stampfl, M. Scheffler, M. Wolf, and G. Ertl, Science **285**, 1042 (1999).
[3] S. Zhao, D.-W. Wang, R. Amal, and L. Dai, Advanced Materials **31**, 1801526 (2019).
[4] G. Higashi, Y. Chabal, G. Trucks, and K. Raghavachari, Applied physics letters **56**, 656 (1990).
[5] S. M. Lee, K. S. Park, Y. C. Choi, Y. S. Park, J. M. Bok, D. J. Bae, K. S. Nahm, Y. G. Choi, S. C. Yu, N.-g. Kim, *et al.*, Synthetic metals **113**, 209 (2000).
[6] R. Díez Muiño and H. Busnengo, *Dynamics of Gas-Surface Interactions: Atomic-level Understanding of Scattering Processes at Surfaces*, Springer Series in Surface Sciences (Springer, 2013).
[7] G. A. Somorjai and Y. Li, *Introduction to surface chemistry and catalysis* (John Wiley & Sons, 2010).
[8] F. Rodriguez-Hernandez, D. C. Tranca, B. M. Szyja, R. A. van Santen, A. Martínez-Mesa, L. Uranga-Piña, and G. Seifert, The Journal of Physical Chemistry C **120**, 437 (2016).
[9] A. Valdes, J. Brillet, M. Grätzel, H. Gudmundsdottir, H. A. Hansen, H. Jonsson, P. Klüpfel, G.-J. Kroes, F. Le Formal, I. C. Man, *et al.*, Physical Chemistry Chemical Physics **14**, 49 (2012).
[10] M. R. Usman, Renewable and Sustainable Energy Reviews **167**, 112743 (2022).
[11] Y. Yürüm, A. Taralp, and T. N. Veziroglu, International journal of hydrogen energy **34**, 3784 (2009).
[12] B. Sakintuna, F. Lamari-Darkrim, and M. Hirscher, International journal of hydrogen energy **32**, 1121 (2007).
[13] A. Kleyn, N. L. Cardozo, and U. Samm, Physical Chemistry Chemical Physics **8**, 1761 (2006).
[14] V. Barabash, G. Federici, R. Matera, A. Raffray, and I. H. Teams, Physica Scripta **1999**, 74 (1999).
[15] G. Federici, H. Wuerz, G. Janeschitz, and R. Tivey, Fusion engineering and design **61**, 81 (2002).
[16] G. Federici, P. Andrew, P. Barabaschi, J. Brooks, R. Doerner, A. Geier, A. Herrmann, G. Janeschitz, K. Krieger, A. Kukushkin, *et al.*, Journal of Nuclear Materials **313**, 11 (2003).
[17] J. Roth, E. Tsitrone, A. Loarte, T. Loarer, G. Counsell, R. Neu, V. Philipps, S. Brezinsek, M. Lehnen, P. Coad, *et al.*, Journal of Nuclear Materials **390**, 1 (2009).
[18] D. Hollenbach and E. Salpeter, The Astrophysical Journal **163**, 155 (1971).
[19] O. Bünermann, H. Jiang, Y. Dorenkamp, A. Kandratsenka, S. M. Janke, D. J. Auerbach, and A. M. Wodtke, Science **350**, 1346 (2015).
[20] Y. Dorenkamp, H. Jiang, H. Köckert, A. Janke, Svenja Mand Kandratsenka, A. M. Wodtke, and O. Bünermann, The Journal of Chemical Physics **148**, 034706 (2018).
[21] S. M. Janke, D. J. Auerbach, A. M. Wodtke, and A. Kandratsenka, The journal of Chemical Physics **143**, 124708 (2018).
[22] M. Kammler, S. M. Janke, , A. Kandratsenka, and A. M. Wodtke, Chemical Physics Letter **683**, 286 (2017).
[23] A. Kandratsenka, H. Jiang, Y. Dorenkamp, S. M. Janke, M. Kammler, A. M. Wodtke, and O. Bünermann, Proceedings of the National Academy of Sciences **115**, 680 (2018).
[24] N. Hertl, R. Martin-Barrios, O. Galparsoro, P. Larrégaray, D. J. Auerbach, D. Schwarzer, A. M. Wodtke, and A. Kandratsenka, The Journal of Physical Chemistry C **125**, 14468 (2021).
[25] O. Galparsoro, R. Péétuya, H. F. Busnengo, J. I. Juaristi, C. Crespos, M. Alducin, and P. Larregaray, Physical Chemistry Chemical Physics **18**, 31378 (2016).
[26] O. Galparsoro, H. F. Busnengo, J. I. Juaristi, C. Crespos, M. Alducin, and P. Larregaray, The journal of Chemical Physics **147**, 121103 (2017).
[27] R. Martin Barrios, O. Galparsoro, A. Martinez Mesa, L. Uranga-Piña, C. Crespos, and P. Larregaray, The Journal of Physical Chemistry C **125**, 14075 (2021).

[28]N. Hertl, A. Kandratsenka, and A. M. Wodtke, Physical Chemistry Chemical Physics **24**, 8738 (2022).
[29]E. Quintas-Sánchez, P. Larregaray, C. Crespos, L. Martin-Gondre, J. Rubayo-Soneira, and J.-C. Rayez, The Journal of chemical physics **137**, 064709 (2012).
[30]E. Quintas-Sánchez, C. Crespos, P. Larrégaray, J. Rayez, L. Martin-Gondre, and J. Rubayo-Soneira, The Journal of Chemical Physics **138**, 024706 (2013).
[31]R. Pétuya, P. Larrégaray, C. Crespos, H. F. Busnengo, and A. E. Martinez, The Journal of Chemical Physics **141**, 024701 (2014).
[32]R. Pétuya, C. Crespos, E. Quintas-Sanchez, and P. Larrégaray, The Journal of Physical Chemistry C **118**, 11704 (2014).
[33]M. Nosir, L. Martin-Gondre, G. A. Bocan, and R. D. Muiño, Physical Chemistry Chemical Physics **19**, 7370 (2017).
[34]I. Goikoetxea, M. Alducin, R. D. Muiño, and J. Juaristi, Physical Chemistry Chemical Physics **14**, 7471 (2012).
[35]I. Goikoetxea, J. Juaristi, R. D. Muiño, and M. Alducin, Physical Review Letters **113**, 066103 (2014).
[36]H. Busnengo, A. Salin, and W. Dong, J. Chem. Phys. **112**, 7641 (2000).
[37]R. A. Olsen, H. F. Busnengo, A. Salin, M. F. Somers, G. J. Kroes, and E. J. Baerends, J. Chem. Phys. **116**, 3841 (2002).
[38]Y. Perdew, J. P.; Wang, Phys. Rev. B **45**, 13244 (1992).
[39]J. P. Perdew, *Electronic Structure of Solids* (Ziesche, P., Eschring, H., Eds.; Akademie-Verlag, Berlin, 1991).
[40]J. I. Juaristi, M. Alducin, R. Diéz-Muino, H. F. Busnengo, and A. Salin, Physical Review Letters **100**, 116102 (2008).
[41]M. Alducin, R. Diéz-Muino, and J. I. Juaristi, Progress in Surface Science **92**, 317 (2017).
[42]M. Blanco-Rey, J. I. Juaristi, R. Díez Muiño, H. F. Busnengo, G. J. Kroes, and M. Alducin, Phys. Rev. Lett. **112**, 103203 (2014).
[43]D. Novko, M. Blanco-Rey, J. I. Juaristi, and M. Alducin, Phys. Rev. B **92**, 201411 (2015).
[44]D. Novko, M. Blanco-Rey, J. I. Juaristi, and M. Alducin, Phys. Rev. B **93**, 245435 (2016).
[45]O. Galparsoro, J. I. Juaristi, C. Crespos, M. Alducin, and P. Larrégaray, The Journal of Physical Chemitry C **121**, 19849 (2017).
[46]P. Saalfrank, Chemical Review **106**, 4116 (2006).
[47]C. Springer, M. Head-Gordon, and J. C. Tully, Surface Science **320**, L57 (1994).
[48]C. Springer and M. Head-Gordon, Chemical Physics **205**, 73 (1996).
[49]R. Scholtz, G. Floss, P. Saalfrank, G. Fuchsel, I. Loncaric, and J. I. Juaristi, Physical Review B **94**, 165447 (2016).
[50]R. Scholtz, S. Lindner, I. Loncaric, J. C. Tremblay, J. I. Juaristi, M. Alducin, and P. Saalfrank, Physical Review B **100**, 245431 (2019).
[51]I. Loncaric, M. Alducin, P. Saalfrank, and J. I. Juaristi, Nuclear Instruments and Methods in Physics Research B **382**, 114 (2016).
[52]G. Füchsel, T. Klamroth, S. Monturet, and P. Saalfrank, Phys. Chem. Chem. Phys. **13**, 8659 (2011).
[53]R. Martin-Barrios, N. Hertl, O. Galparsoro, A. Kandratsenka, A. M. Wodtke, and P. Larrégaray, Physical Chemistry Chemical Physics **24**, 20813 (2022).
[54]M. Pavanello, D. J. Auerbach, A. M. Wodtke, M. Blanco-Rey, M. Alducin, and G.-J. Kroes, J. Phys. Chem. Lett. **4**, 3735 (2013).
[55]G.-J. Kroes, M. Pavanello, M. Blanco-Rey, M. Alducin, and D. J. Auerbach, J. Chem. Phys. **141**, 054705 (2014).